# Materials Advances

Accepted Manuscript

This article can be cited before page numbers have been issued, to do this please use: B. Xu, X. Fu, Z. Huang, C. Zhang and X. Hu, *Mater. Adv.*, 2026, DOI: 10.1039/D6MA00384B.




ROYAL SOCIETY OF CHEMISTRY

rsc.li/materials-advances

View Article Online
DOI: 10.1039/D6MA00384B

# A photosensitizer-drug conjugate for synergistic photodynamic therapy and photo-triggered camptothecin release

Received 00th January 20xx,
Accepted 00th January 20xx

DOI: 10.1039/x0xx00000x

Bowen Xu,[ab] Xuancheng Fu,[ab] Zhiwei Huang,[a] Cijun Zhang,[ab] Xiaoran Hu*[ab]

Combination therapy has emerged as a promising strategy to enhance treatment efficacy at reduced doses and overcome the limitations of monotherapy by harnessing complementary therapeutic modalities, while external stimulus-controlled therapeutic activation can localize therapeutic activity to tumors and reduce systemic toxicity. Here, we present a chemo-photodynamic combination nanotherapy strategy based on a red light-responsive photosensitizer-drug conjugate. This prodrug integrates the photosensitizer 5-mono(4-carboxyphenyl)-10,15,20-triphenylporphine (TPP) with an anticancer drug camptothecin (CPT) through a singlet oxygen-cleavable thioketal linker. The prodrug exhibited minimal dark toxicity in vitro and was readily encapsulated into PLGA-PEG nanoparticles, affording nanoparticles exhibited uniform morphology, high stability, and efficient cellular uptake. Upon red light irradiation, TPP generates singlet oxygen ($^1O_2$) to induce photodynamic cytotoxicity and simultaneously cleaves the thioketal linker, triggering the controlled release of CPT. The intrinsic PDT cytotoxicity of photo-generated $^1O_2$, together with CPT released via $^1O_2$-mediated thioketal cleavage synergistically enhanced cytotoxicity in photo-irradiated HeLa cells compared with either PDT or chemotherapy alone. Collectively, this study demonstrates a chemo-photodynamic combination nanotherapy strategy that enables red-light-guided, spatiotemporal control of cancer therapy.



## Introduction

Cancer remains one of the leading causes of mortality worldwide, yet conventional cancer therapies are often limited by suboptimal therapeutic efficacy, off-target toxicity in healthy tissues, and acquired drug resistance that diminishes long-term efficacy.[1, 2] Spatiotemporally controlled treatment can localize therapeutic activity to the tumors to reduce nonspecific exposure of healthy tissues,[3–5] while combination therapy harnesses complementary therapeutic modalities to enhance efficacy at reduced doses, thereby reducing systemic toxicity relative to monotherapy and mitigating the emergence of drug resistance.[6–8]

Photodynamic therapy (PDT) is a light-activated treatment in which a photosensitizer, under irradiation at an appropriate wavelength of light, is photoexcited and transfers energy (or electrons) to generate cytotoxic reactive oxygen species (most commonly singlet oxygen ($^1O_2$); type II PDT) that induce localized oxidative damage in the light-irradiated regions.[9–12] Because PDT operates primarily via oxidative damage to biomolecules and cellular components (e.g., membranes),[13] it is mechanistically orthogonal to many conventional therapies and therefore enables complementary and potentially synergistic treatment efficacy and is less susceptible to common drug-resistance mechanisms. Accordingly, combining PDT with conventional cancer therapy modalities is a promising strategy to achieve therapeutic synergy and overcome limitations associated with monotherapy.[14–19]

A prodrug is a pharmacologically inactive compound that, upon administration, is enzymatically or chemically converted to release active therapeutic agents at targeted sites.[20–22] Building upon this concept, stimuli-responsive prodrug platforms have been developed to achieve spatiotemporally controlled drug activation by incorporating stimulus-cleavable linkers that respond to tumor-associated microenvironmental cues (e.g., acidic pH, [23–25] elevated ROS, [26, 27] overexpressed enzymes, [28, 29] high intracellular glutathione (GSH), [30, 31] and hypoxia[32, 33]) or externally applied triggers (e.g., light irradiation, [34–38] ultrasound, [39, 40] and ionizing radiation[41–43]). By integrating responsive chemistry with prodrug design, these systems offer improved systemic stability and tumor-selective drug release. However, systems that rely on endogenous tumor-associated stimuli often suffer from insufficient specificity and tumor heterogeneity, as these triggers may also be present at low levels in normal tissues, leading to undesired drug activation and limited control over activation selectivity. Photo-cleavage chemistry has been widely adopted to regulate prodrug activation[44] and increasing efforts have been devoted to developing photo-cleavage chemistry with red-shifted excitation wavelengths for enhanced tissue penetration.[45–47] An emerging strategy in photo-mediated cleavage chemistry leverages PDT-generated reactive oxygen species (ROS) to trigger preprogrammed oxidative reactions, resulting in cascade bond cleavage and drug release.[48–52] Such a PDT-mediated strategy significantly diversifies and expands the structural and functional scope of photocleavage chemistry,[53] given the rich library of photosensitizers responsive to wavelengths spanning the visible to the near-infrared. Of particular interest are thioketal linkers that undergo oxidative cleavage and have been used to construct ROS-activable prodrug systems.[54–61] In this context, covalent conjugation of a chemotherapeutic agent with a photosensitizer through a ROS-responsive linker enables photo-activation of prodrugs using longer-wavelength light, while offering synergy between chemo and photodynamic therapy modalities.

Nanocarriers offer a number of advantages over the direct usage of small-molecule drugs, such as protection of payloads from premature degradation, solubilizing hydrophobic drugs, reduced nonspecific drug exposure, and tunable control over

[a] Department of Chemistry, Syracuse University, Syracuse, New York, 13244, United States.
[b] BioInspired Institute, Syracuse University, Syracuse, New York, 13244, United States.

View Article Online
DOI: 10.1039/D6MA00384B

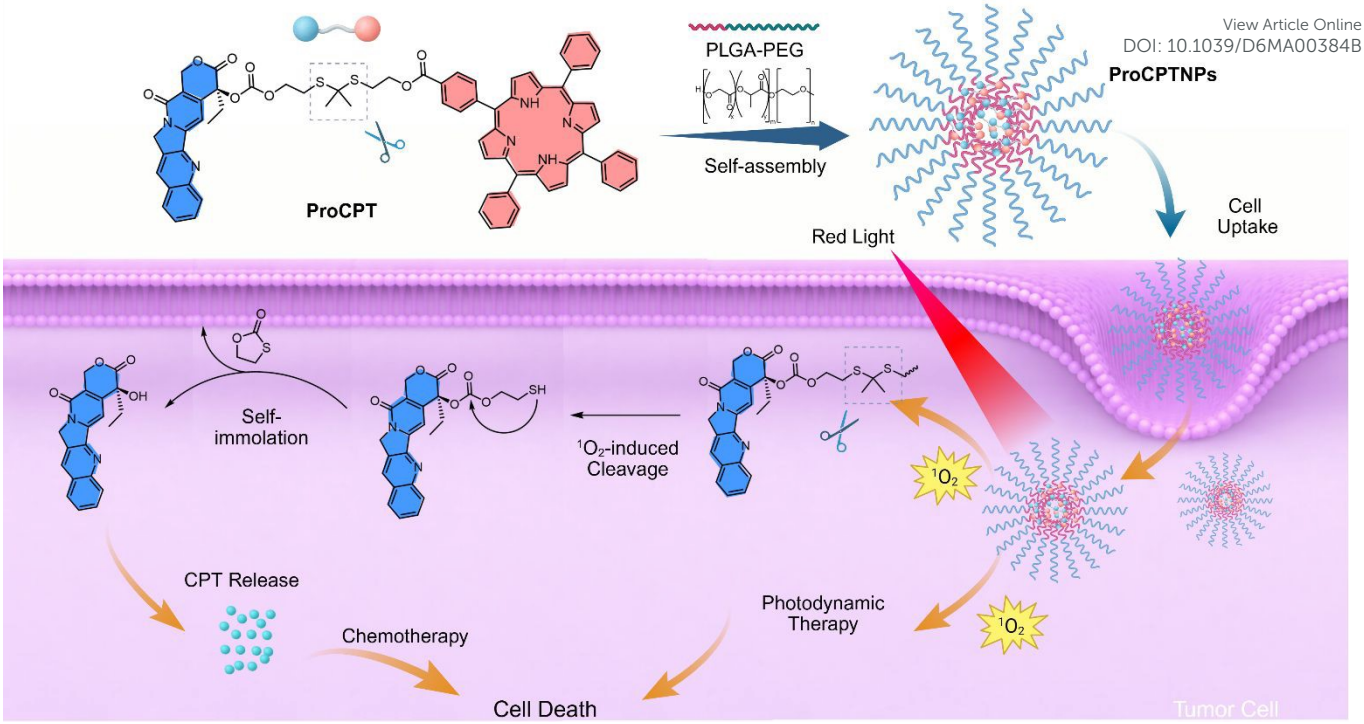


**Fig. 1** Schematic illustration of the preparation of **ProCPTNPs** and its therapeutic effects.

cellular uptake, and so on.[62–64] For example, PLGA–PEG is a widely used biocompatible diblock copolymer comprising a hydrophilic PEG segment and a biodegradable PLGA segment, and can readily self-assemble into core-shell nanoparticles to encapsulate hydrophobic drugs under appropriate formulation conditions.[65] Such PLGA–PEG nanoformulations have been extensively employed to improve pharmacokinetics and biodistribution, thereby enhancing therapeutic performance in biological environments.[66, 67]

Herein we report a chemo-photodynamic combination nanotherapy strategy based on a photosensitizer-drug conjugate comprising an anticancer drug CPT conjugated to a porphyrin derivative (the photosensitizer) through a $^1O_2$-cleavable thioketal linker (Fig. 1). This conjugate exhibits minimal dark toxicity in vitro and can be stably encapsulated into PLGA-PEG nanoparticles, which exhibited uniform morphology, high stability, and efficient cellular uptake. Upon red light irradiation (> 600 nm), the photosensitizer TPP,[68–70] generates $^1O_2$ and simultaneously induces PDT cytotoxicity while cleaving the thioketal linker to release CPT with restored chemotherapeutic toxicity. Combination index–fraction affected (CI–Fa) analysis demonstrates synergistic effects of this combined chemo-PDT nanotherapy system, enabled by light-triggered $^1O_2$ generation that drives phototoxicity and prodrug activation. By combining synergistic chemo-PDT cytotoxicity with light-controlled (> 600 nm) spatiotemporal resolution, this nanotherapy platform holds promise to improve localized therapeutic efficacy while potentially mitigating systemic toxicity.

## Materials and methods

**Synthesis of $^1O_2$-responsive prodrug ProCPT**

The synthetic procedure for **ProCPT** is illustrated in Scheme 1 (see Supporting Information for synthetic details). Briefly, a $^1O_2$-responsive thioketal diol linker (Compound **2**) was synthesized from 2-mercaptoethanol through sequential thioketal formation and deprotection steps. CPT was reacted with triphosgene in the presence of DMAP and coupled with the thioketal linker to afford the CPT-linker intermediate (Compound **3**). Compound **3** was conjugated to 5-mono(4-carboxyphenyl)-10,15,20-triphenylporphyrin (TPP-COOH) via EDC/DMAP-mediated coupling to yield the target prodrug **ProCPT**. Synthetic intermediates and products were structurally confirmed by $^1$H and $^{13}$C NMR and high-resolution mass spectrometry.

**Preparation of ProCPTNPs and TPPNPs**

**ProCPT** (1 mg) or TPP (0.5 mg) and PLGA (10 kDa)–mPEG (5 kDa) (10 mg) were dissolved in THF (1 mL). The resulting solution was rapidly added into deionized water (10 mL) within 30 s under stirring (1000 rpm). The organic solvent (THF) was removed under reduced pressure to ensure complete solvent removal. The obtained nanoparticles were concentrated to 1 mg mL$^{-1}$ and stored in dark at 4 °C.

**Size, zeta potential and colloidal stability measurements**

Dynamic light scattering (DLS) measurements were carried out using a Zetasizer Nano ZS (Malvern Panalytical, UK) equipped with a 173° backscattering detector. All measurements were performed at 25 °C, and hydrodynamic diameters were reported as intensity-weighted size distributions. Samples were diluted to an appropriate scattering intensity in PBS prior to

View Article Online
DOI: 10.1039/D6MA00384B

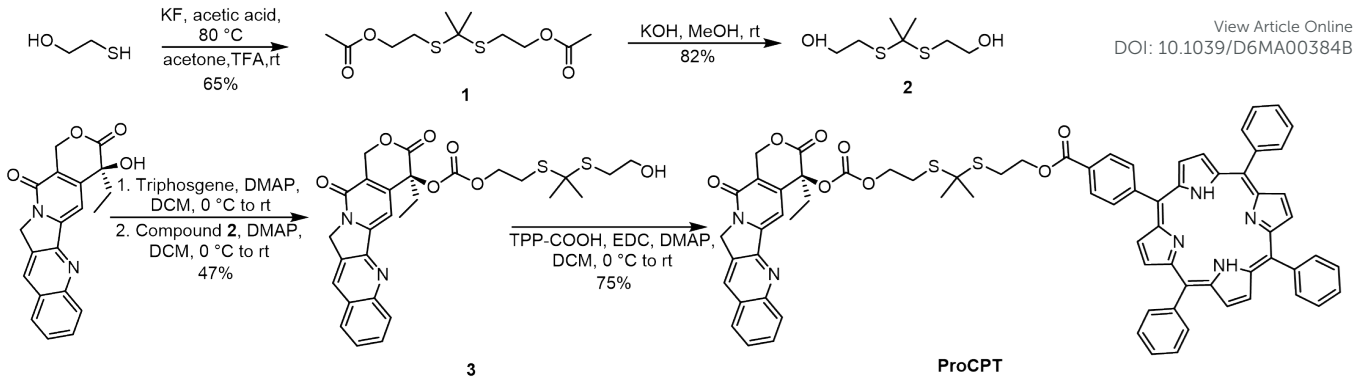


**Scheme 1** Synthesis of $^1O_2$-responsive prodrug **ProCPT**.

measurement. Each sample was measured in triplicate (n = 3), and the data are presented as mean ± standard deviation. Zeta potential values were determined using the same instrument with folded capillary cells.

Colloidal stability was assessed by incubating **ProCPTNPs** and **TPPNPs** in Roswell Park Memorial Institute (RPMI)-1640 medium supplemented with 10% fetal bovine serum (FBS) at 37 °C under gentle shaking. At predetermined time points, changes in hydrodynamic diameter were monitored by DLS.

**UV–vis and fluorescence spectroscopy**

UV–vis absorption spectra were recorded using a Cary 60 UV–vis spectrophotometer (Agilent Technologies, USA). **ProCPT** and **ProCPTNPs** were dispersed in PBS at a concentration of 5 μM (equivalent to 66.5 μg mL$^{-1}$ for **ProCPTNPs**) and measured at room temperature.

Fluorescence spectra were recorded using a Cary Eclipse fluorescence spectrophotometer (Agilent Technologies, USA). Samples were excited at 600 nm, and emission spectra were collected over the range of 620–800 nm.

**In vitro singlet oxygen generation**

Singlet Oxygen Sensor Green (SOSG)[71, 72] was used as a fluorescent probe for singlet oxygen ($^1O_2$) detection. Briefly, 13.3 μg mL$^{-1}$ **ProCPTNPs** (i.e., 1 μM **ProCPT**) in PBS was mixed with SOSG (5 μM) and irradiated with red light (> 600 nm, 40 mW cm$^{-2}$) for predetermined time intervals. The fluorescence intensity of SOSG at 530 nm ($\lambda_{ex}$ = 488 nm) was recorded using a Cary Eclipse fluorescence spectrophotometer (Agilent Technologies, USA). Each experiment was performed in triplicate (n = 3), and the data are presented as mean ± standard deviation.

**CPT release study**

A PBS solution of **ProCPT** (5 μM) was irradiated with red light (> 600 nm, 40 mW cm$^{-2}$) for predetermined time intervals and subsequently incubated overnight at room temperature to allow complete reaction. The release of CPT was analysed by high-performance liquid chromatography (HPLC).

HPLC analysis was performed using a Shimadzu LC–20 system (Shimadzu, Japan) equipped with a Shimadzu Nexcol C18 column (5 μm, 4.6 × 250 mm). The mobile phase consisted of (A) acetonitrile containing 0.1% trifluoroacetic acid (TFA) and (B) water containing 0.1% TFA. A linear gradient was applied from 5% to 95% acetonitrile over 15 min at a flow rate of 1.0 mL min$^{-1}$. The column temperature was maintained at 25 °C, and detection was carried out at 254 nm using a UV detector.

**Cell culture**

HeLa cells were cultured in RPMI-1640 containing 10% FBS and 1% penicillin/streptomycin and maintained at 37 °C in a humidified atmosphere containing 5% $CO_2$.

**Cellular uptake**

HeLa cells (1 × 10$^4$) were seeded in 96-well plates and cultured overnight to allow adherence. The medium was then replaced with fresh RPMI-1640 containing **ProCPTNPs** (100 μg mL$^{-1}$), and the cells were incubated at 37 °C for 0, 4, 8 and 12 h. Subsequently, LysoTracker™ Deep Red (75 nM in RPMI-1640 medium) was added to the cells and incubated for 30 min at 37 °C to stain lysosomes. The nuclei were counterstained with Hoechst 33342 (5 μg mL$^{-1}$ in RPMI-1640 medium) for 10 min. After staining, cells were carefully washed three times with ice-cold PBS (1×) to remove excess dyes.

Fluorescence images were acquired using a Zeiss LSM 980 Airyscan 2 confocal super resolution microscope (Carl Zeiss, Germany) equipped with a GaAsP detector array. Excitation wavelengths were set at 405 nm for Hoechst 33342, 633 nm for LysoTracker™ Deep Red, and 561 nm for the **ProCPTNPs** fluorescence channel. Images were captured using a Plan-Apochromat 20×/0.8 objective lens. Detector settings, laser power, and acquisition parameters were kept constant across all samples to ensure comparability.

**Measurement of intracellular ROS generation**

HeLa cells (1 × 10$^4$) were seeded in 96-well plates and cultured overnight to allow adherence. Cells were then treated with either PBS (control) or **ProCPTNPs** (100 μg mL$^{-1}$ in RPMI-1640 medium) and incubated at 37 °C for 12 h. After incubation, the cells were washed three times with PBS (1×) and subsequently treated with 2′,7′-dichlorodihydrofluorescein diacetate ($H_2$DCFDA)[73] (20 μM in RPMI-1640 medium) for 20 min at 37 °C. The cells were then irradiated with light (> 600 nm, 40 mW cm$^{-2}$) for 5 min. After irradiation, the cells were washed three times with PBS (1×), and the fluorescence signals derived from

View Article Online
DOI: 10.1039/D6MA00384B

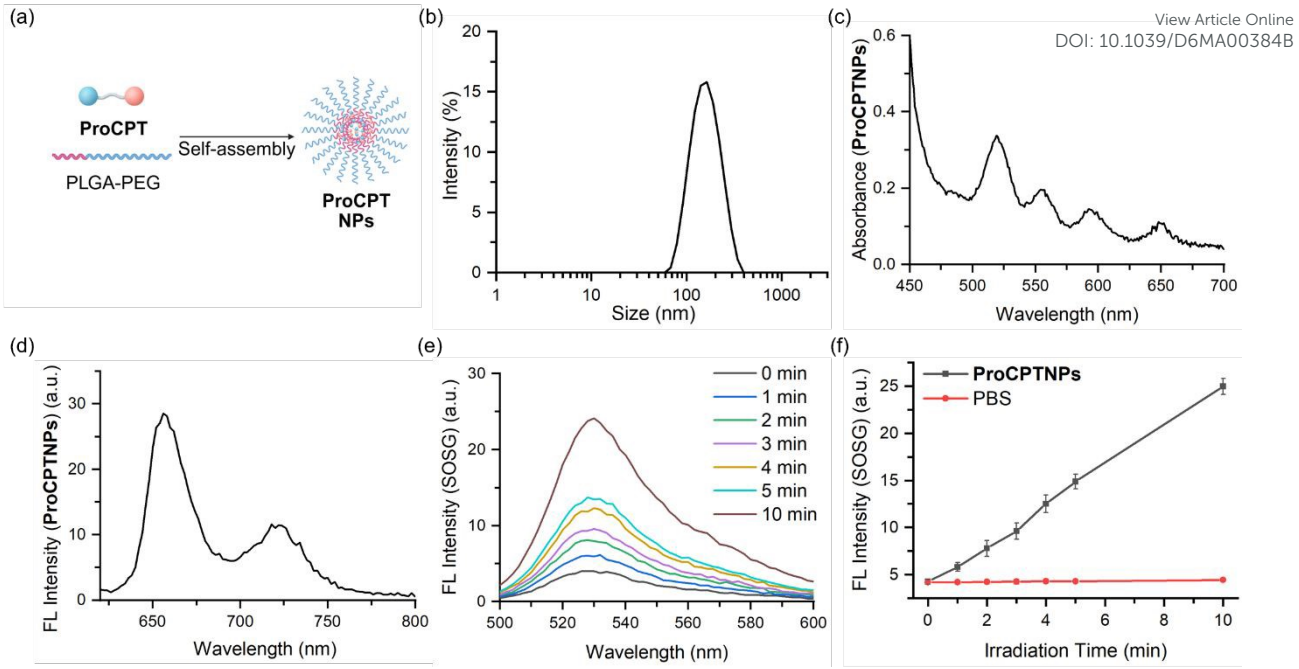


**Fig. 2** Preparation and characterization of **ProCPTNPs**. (a) Schematic illustration of the preparation of **ProCPTNPs**. (b) The size distribution of **ProCPTNPs** measured by DLS. (c) Absorption spectra of **ProCPTNPs** in PBS buffer. (d) Fluorescence spectra of **ProCPTNPs** in PBS buffer. (e) Generation of $^1O_2$ from **ProCPTNPs** as a function of light irradiation time, determined by SOSG assay. (f) The changes in the fluorescence intensity of SOSG (emission peak = 530 nm) with or without **ProCPTNPs** under light irradiation. Irradiation conditions: > 600 nm, 40 mW cm$^{-2}$.

oxidized 2',7'-dichlorofluorescein (DCF) were collected. Excitation and emission were set at 488 nm and 525 ± 20 nm for DCF detection.

**Cytotoxicity test**

HeLa cells were seeded in 96-well plates at a density of 5,000 cells per well and incubated for 24 h to allow cell attachment. Subsequently, cells were treated with different concentrations of **ProCPTNPs** or **TPPNPs**. After 12 h of incubation, the **ProCPTNPs** and **TPPNPs** groups were exposed to light irradiation (> 600 nm, 40 mW cm$^{-2}$) for 15 min. For the chemotherapy group, **ProCPTNPs** were added to the cells immediately after light irradiation under the same conditions (> 600 nm, 40 mW cm$^{-2}$, 15 min). After a total culture time of 48 h, the supernatant was replaced with 100 µL of thiazolyl blue (MTT) solution (0.5 mg mL$^{-1}$ in RPMI-1640 medium) and incubated at 37 °C for 4 hours. The supernatant was removed, 100 µL of DMSO was added to dissolve the formazan crystals, and the plate was shaken for 60 seconds. Absorbance at 490 nm was measured using a microplate reader, and the viability of the blank control group was set as 100% for normalization. Each experimental condition was performed in sextuplicate (n = 6).

## Results and discussion

The photosensitizer TPP was covalently linked to CPT through a $^1O_2$-cleavable thioketal linker, temporarily suppressing the intrinsic cytotoxicity of CPT in the prodrug state (**ProCPT**). The resulting hydrophobic prodrug was subsequently co-assembled with PLGA-PEG amphiphiles to construct a stimuli-responsive nanoplatform (**ProCPTNPs**) (Fig. 2a), ensuring structural stability in aqueous media while mitigating premature drug leakage under physiological conditions. Upon red light irradiation, TPP efficiently generates $^1O_2$, which induces cleavage of the thioketal bond and triggers the on-demand activation of CPT. TPP was selected not only for its high $^1O_2$ quantum yield, but also for its hydrophobic porphyrin framework, which promotes efficient packing of the hydrophobic prodrug and avoids undesired interaction with cells in the encapsulated form.

DLS measurements confirmed that **ProCPTNPs** exhibited a hydrodynamic diameter of approximately 156.4 nm (Fig. 2b) with a surface charge of ~-17.8 mV. The nanoparticles displayed a narrow size distribution with a low polydispersity index (PDI) of 0.091. Scanning electron microscopy (SEM) images (Fig. S1) further revealed well-defined spherical morphology with a size range consistent with that indicated by DLS. Moreover, **ProCPTNPs** demonstrated excellent colloidal stability under physiological conditions, as negligible size changes were observed during long-term storage (~ one week) in PBS (pH 7.4) (Fig. S2).

The optical and photodynamic properties of **ProCPTNPs** were systematically evaluated. Their UV–vis absorption spectra displayed characteristic peaks at around 550–650 nm region, originating from the porphyrin chromophore of TPP (Fig. 2c, Fig. S5). In addition, a distinct emission peak of TPP was observed at around 680 nm (Fig. 2d). To assess the $^1O_2$ generation capability of **ProCPTNPs**, singlet oxygen probe SOSG was employed as a fluorescent probe. Upon irradiation with red light, the SOSG emission at 530 nm gradually increased in the solution of **ProCPTNPs** (Fig. 2e). Quantitative analysis of SOSG emission at 530 nm revealed a 4.3-fold enhancement after 10 min of

View Article Online
DOI: 10.1039/D6MA00384B

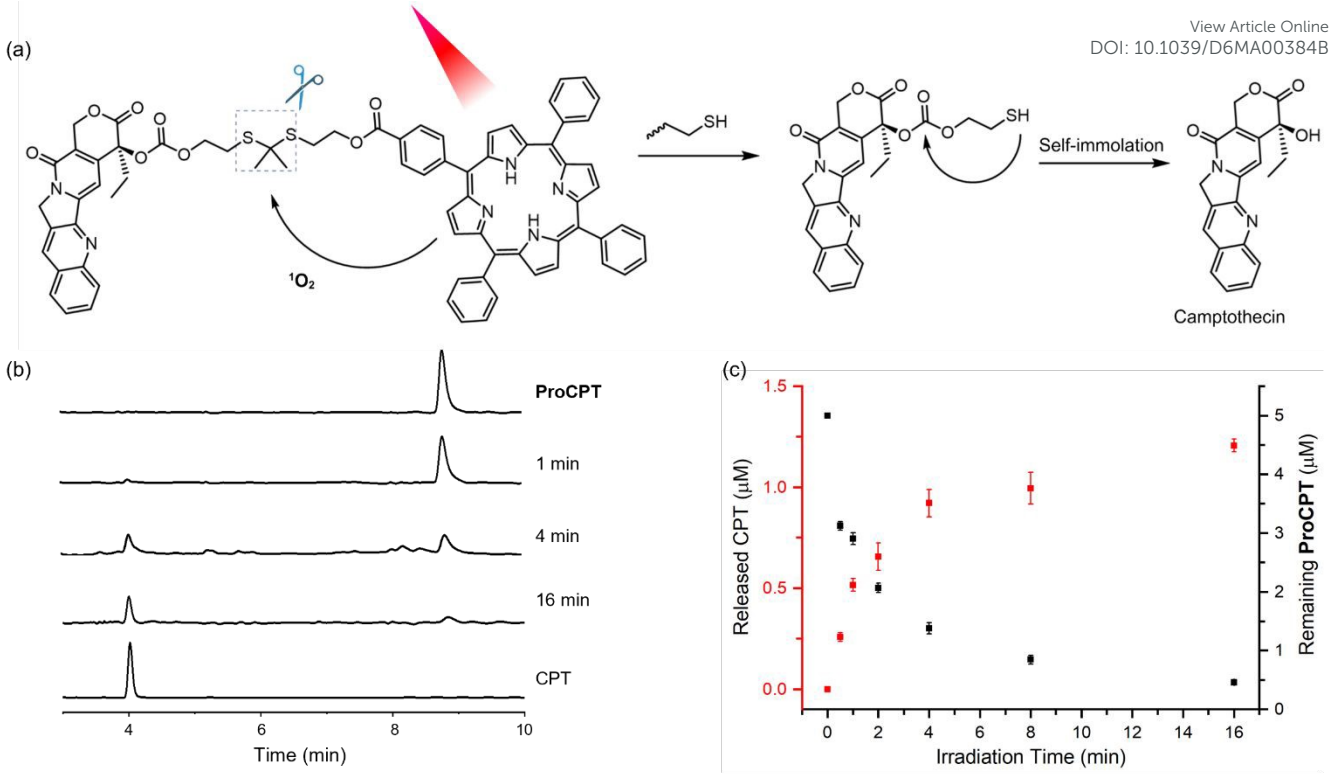


**Fig. 3** (a) Schematic illustration of PDT-mediated CPT release from **ProCPT**. (b) HPLC profiles of **ProCPT** (5 μM) as a function of light irradiation durations (0–16 min), compared against a standard solution of CPT (5 μM, bottom trace). (c) Photo-triggered release of CPT from **ProCPT** as a function of light irradiation monitored by HPLC. Light irradiation conditions: > 600 nm, 40 mW $cm^{-2}$. All photo-irradiated samples were kept at room temperature overnight before HPLC analysis to ensure the completion of cyclization-elimination cascade.

irradiation (Fig. 2f, S6), confirming the efficient $^1O_2$ generation capacity of **ProCPTNPs**.

The photo-generated reactive $^1O_2$ from **ProCPT** efficiently cleaves the thioketal linker within the prodrug, thereby triggering a cascade cyclization-elimination reaction to release free CPT (Fig. 3a). HPLC analysis revealed that, after 16 min of irradiation, the characteristic peak of **ProCPT** (retention time, $t_R$ = 8.75 min) disappeared, accompanied by the emergence of a new elution peak at $t_R$ = 3.95 min which matches the free CPT, thereby confirming the successful photo-controlled CPT release (Fig. 3b). Quantitative analysis demonstrated that ~1.2 μM CPT was released from 5 μM **ProCPT** after 16 min irradiation and overnight incubation, corresponding to a release percentage of ~24% (Fig. 3c).

We next evaluated the cellular uptake and photodynamic activity of **ProCPTNPs** in HeLa cells. After co-incubation with **ProCPTNPs**, cellular internalization was visualized using confocal laser scanning microscopy (CLSM). As the incubation time increased, the intracellular fluorescence from **ProCPT** progressively intensified (Fig. 4a, S7; **ProCPT** fluorescence depicted in green; $\lambda_{ex}$ = 561 nm; $\lambda_{em}$ = 600–630 nm), indicating time-dependent cellular uptake of **ProCPTNPs**, with the mean fluorescence intensity reaching 2.1-fold at 8 h (Fig. 4b). The PLGA–PEG nanoparticles (~150 nm) exhibit a narrow size distribution consistent with previously reported PLGA-based systems and are therefore expected to be internalized by cells through endocytosis.[74, 75] When lysosomes were stained with LysoTracker™ Deep Red, the fluorescence signal (depicted in red) showed clear colocalization with that of **ProCPT** after 8 h of incubation, suggesting lysosomal involvement and supporting endo–lysosomal trafficking following cellular uptake. The acidic lysosomal microenvironment is expected to promote the degradation of PLGA nanoparticles, thereby facilitating the release of encapsulated hydrophobic cargo molecules.[64] More importantly, lysosomes are known to be highly vulnerable organelles to photodynamic damage, which may further potentiate the therapeutic efficacy of **ProCPTNPs**.

Intracellular ROS production triggered by **ProCPTNPs** upon red light irradiation was further examined using $H_2$DCFDA as a fluorescent probe. $H_2$DCFDA is non-fluorescent until oxidized by ROS to yield the green-fluorescent DCF.[73] As shown in confocal fluorescence images (Fig. 4c), negligible DCF fluorescence was observed in HeLa cells incubated with PBS or **ProCPTNPs** under dark conditions. In contrast, strong green fluorescence emerged in **ProCPTNPs**-treated cells upon red light irradiation. Quantitative analysis demonstrated that DCF fluorescence intensity in irradiated cells was approximately 25-fold higher than in non-irradiated controls (Fig. 4d). These findings

View Article Online
DOI: 10.1039/D6MA00384B



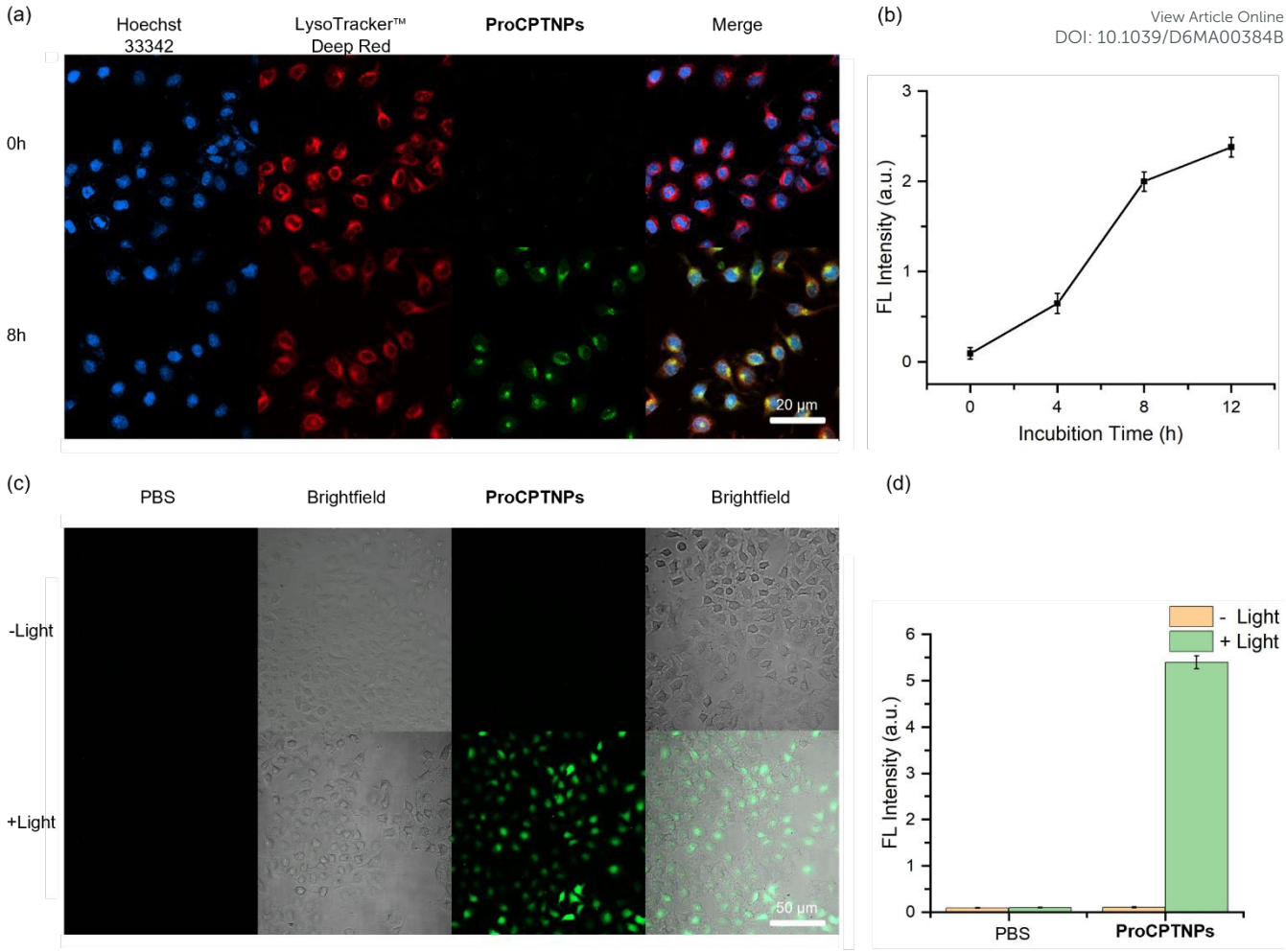


**Fig. 4** (a) Confocal fluorescence images and (b) mean fluorescence intensity (MFI) of HeLa cells treated with **ProCPTNPs** for 0, 4, 8 and 12 h. Arbitrary colors are shown in the figure for visual clarity only and do not represent the actual fluorescence emission colors: blue, Hoechst 33342 (nucleus); red, LysoTracker™ (lysosomes); green, **ProCPTNPs**. Scale bar: 20 μm. (c) Confocal fluorescence/brightfield overlay images and (d) MFI of HeLa cells treated with **ProCPTNPs** for 12 h, followed by staining with $H_2$DCFDA and red light photoirradiation (> 600 nm, 40 mW $cm^{-2}$) for 5 min. DCF fluorescence is indicated in green. Scale bar: 50 μm.

unambiguously confirm that **ProCPTNPs** are capable of selectively generating substantial intracellular ROS in areas exposed to red light irradiation.

The chemo-PDT combination therapy of **ProCPTNPs** against HeLa cells was evaluated using the MTT assay. Such combination strategies are designed to enhance therapeutic efficacy through complementary mechanisms while reducing the likelihood of resistance associated with monotherapy. For comparison, nanoparticles containing only the TPP photosensitizer (**TPPNPs**) were also prepared. Without red light irradiation, both **ProCPTNPs** and **TPPNPs** exhibited negligible cytotoxicity, with cell viability remaining above 80%, confirming their good biocompatibility in the dark (Fig. 5a, b). Upon red light irradiation (> 600 nm, 40 mW $cm^{-2}$, 15 min), both groups showed enhanced cytotoxicity, while more significant photo-induced toxicity was observed for the **ProCPTNPs** group ($IC_{50}$ = 0.95 ± 0.05 μM) compared with the **TPPNPs** ($IC_{50}$ = 6.0 ± 0.21 μM). At a fixed concentration of 3 μM, light irradiation induced only a moderate decrease in MTT viability (50 %) for the **TPPNPs** group, whereas **ProCPTNPs** caused a markedly increased cytotoxicity (MTT viability = 23 %). We attribute the enhanced cell-killing capability of **ProCPTNPs** to a synergistic effect between photodynamic oxidative damage and PDT-mediated prodrug activation (Fig. 5b). In addition, exposure of cells to the same light conditions in the absence of nanoparticles induced negligible cytotoxicity, confirming that the observed phototoxicity originated from the photo-responsive nanoparticles. Collectively, these results demonstrate that **ProCPTNPs** effectively integrate photodynamic therapy and chemotherapy, achieving superior cancer cell killing with minimal dark toxicity.

In another controlled experiment, chemo-PDT combination therapy (**ProCPTNPs**) was compared to a chemotherapy-only condition, in which **ProCPTNPs** were irradiated ex-situ in a vial and then this pre-activated solution was incubated with HeLa cells (Figure 5a and 5b). This ex-situ irradiation allows PDT-mediated prodrug activation in the nanoparticles, yet cells were not subjected to the PDT oxidative environment due to the

View Article Online
DOI: 10.1039/D6MA00384B

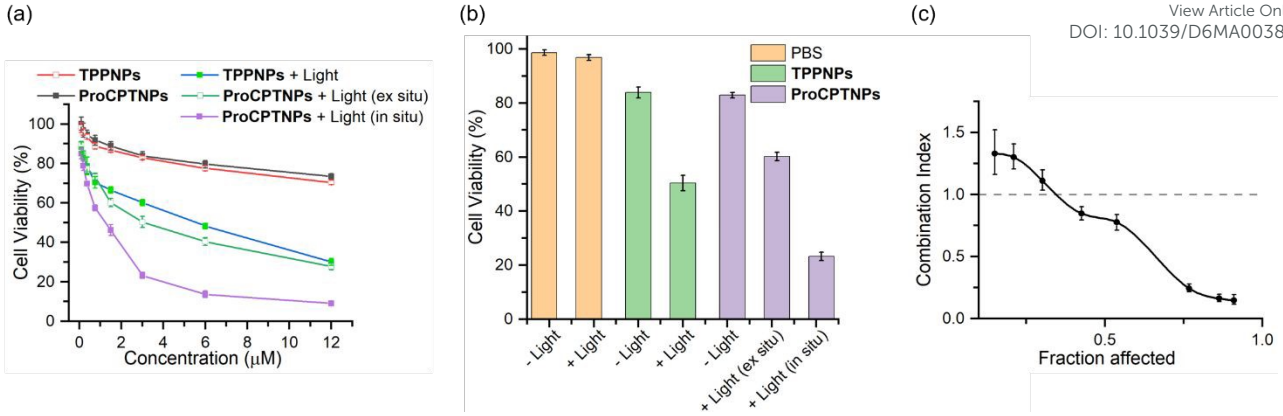


Fig. 5 (a) Cell viability following different treatments, as measured by the MTT assay. Data are shown as mean ± SD (n = 6). (b) Bar graphs showing cell viability under different treatment conditions: PBS (negative control), **TPPNPs** (PDT only), and **ProCPTNPs** (ex situ: **ProCPTNPs** solutions were irradiated in a vial before adding into the cell culture medium, isolating the cytotoxic effect of chemotherapy from PDT; in situ: **ProCPTNPs** were added into the cell culture medium and then irradiated for combination therapy). Concentration of TPP/**ProCPT** = 3 μM. Data are presented as mean ± SD (n = 6). (c) Combination index (CI) analysis of the interaction between photodynamic therapy **TPPNPs** and chemotherapy CPT in the **ProCPTNPs** combination system. The error bars represent the 95% confidence intervals for the CI values. CI > 1 indicates antagonism, CI < 1 indicates synergism, and CI = 1 indicates an additive effect.

short lifetimes of ROS species. The suboptimal therapeutic effect ($IC_{50}$ = 3.2 ± 0.31 μM) of this chemotherapy-only control group underscores the direct contribution from the PDT cytotoxicity that is in synergy with the photo-released drugs.

The synergistic interaction between CPT and PDT was quantitatively evaluated using the Chou–Talalay method.[76] The combination index (CI) analysis was performed at a fixed molar ratio of CPT to TPP (~1:1), which was maintained across all tested concentrations based on the nanoparticle formulation. As shown in Fig. 5c, the CI–Fa curve remained consistently below 1.0 over a broad fraction affected (Fa) range, confirming a synergistic rather than additive effect. At the 50% inhibitory fraction Fa = 0.5, the CI value was approximately 0.80, indicating that a reduced dose of each modality was sufficient to achieve half-maximal inhibition in combination. With increasing Fa, the CI values declined further, reaching below 0.5 at higher effect levels, which demonstrates a dose-dependent enhancement of synergy. This effect arises from the dual function of the **ProCPTNPs** system, where red-light-triggered ROS generation not only induces direct PDT cytotoxicity but also cleaves the thioketal linker to release CPT in situ. Mechanistically, PDT-induced cytotoxicity arises from the generation of reactive oxygen species that oxidatively damage cellular lipids, proteins, nucleic acids, and organelle membranes.[77–79] In contrast, the anticancer agent CPT exerts its therapeutic activity through inhibition of DNA topoisomerase I, stabilizing the Topo I–DNA cleavage complex and inducing replication-associated DNA damage.[80] Owing to their mechanistically distinct yet complementary modes of action, the combination of PDT and CPT has the potential to overcome the intrinsic limitations of each monotherapy. Collectively, these findings demonstrate that **ProCPTNPs** enable spatiotemporally controlled chemo-photodynamic synergy, achieving enhanced therapeutic efficacy at reduced doses compared with either modality alone.

## Conclusions

In conclusion, we have developed a red-light-responsive prodrug nanoplatform **ProCPTNPs** that rationally integrates PDT and CPT chemotherapy within a single molecular construct via a $^1O_2$-cleavable, self-immolative thioketal linker. Because both the PDT cytotoxicity and prodrug activation are contingent upon PDT-mediated ROS production, therapeutic activity of this nanomedicine system is spatiotemporally controlled by deep-penetrating red light, thereby confining cytotoxic effects on demand. Additionally, the PDT and chemotherapy cooperate to damage tumor cells via orthogonal yet complementary mechanisms PDT-driven oxidative damage coupled with drug-mediated DNA disruption, resulting in enhanced cytotoxic pressure beyond that achievable by either monotherapy alone. Consistent with this dual-modality mechanism, combination index analysis demonstrated significant synergy between PDT-induced oxidative stress and CPT-mediated topoisomerase I inhibition, particularly at intermediate effect levels (CI (Fa = 0.5) ≈ 0.80). Overall, this study reports a rationally designed photosensitizer-drug conjugate strategy harnessing the combined effects of chemo-photodynamic therapy, while enabling externally controlled therapeutic efficacy by red light to reduce systemic exposure.

## Author contributions

B. Xu led the study and contributed to the manuscript writing. X. Fu, Z. Huang and C. Zhang contributed to the experimental work. X. Hu oversaw the project, secured funding and resources, and contributed to the manuscript writing.

## Conflicts of interest

There are no conflicts to declare.

View Article Online
DOI: 10.1039/D6MA00548B

## Data availability

Supplementary information: experimental details, supporting figures, synthetic procedures, UV–vis, fluorescence, HPLC, and NMR spectra.

## Acknowledgements

Financial support from Syracuse University (SU) is gratefully acknowledged. We thank Professor Mathew M. Maye (Syracuse University) for generous access to DLS instrument. We thank Professor Eric Benjamin Finkelstein (Syracuse University) for assistance with SEM measurements. The authors acknowledge that elements of Fig. 1–3 and TOC were Created in BioRender. https://www.BioRender.com (Created in BioRender). Xu, B. (2026) https://BioRender.com/it79m6q
https://BioRender.com/upcp9pf
https://BioRender.com/l9ox8pv

## References

1 C. Holohan, S. Van Schaeybroeck, D. B. Longley and P. G. Johnston, *Nat. Rev. Cancer*, 2013, **13**, 714–726. https://doi.org/10.1038/nrc3599
2 U. Anand, A. Dey, A. K. Singh Chandel, R. Sanyal, A. Mishra, D. K. Pandey, V. De Falco, A. Upadhyay, R. Kandimalla, A. Chaudhary, J. K. Dhanjal, S. Dewanjee, J. Vallamkondu and J. M. Pérez de la Lastra, *Genes Dis.*, 2023, **10**, 1367–1401. https://doi.org/10.1016/j.gendis.2022.02.007
3 J. Kost and R. Langer, *Trends Biotechnol.*, 1992, **10**, 127–131. https://doi.org/10.1016/0167-7799(92)90194-Z
4 T. L. Rapp and C. A. DeForest, *Adv. Drug Deliv. Rev.*, 2021, **171**, 94–107. https://doi.org/10.1016/j.addr.2021.01.009
5 X. Fu and X. Hu, *ACS Appl. Bio Mater.*, 2024, **12**, 8040–8058. https://doi.org/10.1021/acsabm.4c00150
6 P. Huang, D. Wang, Y. Su, W. Huang, Y. Zhou, D. Cui, X. Zhu and D. Yan, *J. Am. Chem. Soc.*, 2014, **136**, 11748–11756. https://doi.org/10.1021/ja505212y
**7** Z. Wang, R. Ma, L. Yan, X. Chen and G. Zhu, *Chem. Commun.*, 2015, **51**, 11587–11590. https://doi.org/10.1039/C5CC04376J
8 W. Fan, B. Yung, P. Huang and X. Chen, *Chem. Rev.*, 2017, **117**, 13566–13638. https://doi.org/10.1021/acs.chemrev.7b00258
9 W. Fan, P. Huang and X. Chen, *Chem. Soc. Rev.*, 2016, **45**, 6488–6519. https://doi.org/10.1039/c6cs00616g
10 R. An, X. Cheng, S. Wei, Y. Hu, Y. Sun, Z. Huang, H. Y. Chen and D. Ye, *Angew. Chem. Int. Ed.*, 2020, **59**, 20636–20644. https://doi.org/10.1002/anie.202009141
11 A. P. Castano, P. Mroz and M. R. Hamblin, *Nat. Rev. Cancer*, 2006, **6**, 535–545. https://doi.org/10.1038/nrc1894
12 Z. Zhou, J. Song, L. Nie and X. Chen, *Chem. Soc. Rev.*, 2016, **45**, 6597–6626. https://doi.org/10.1039/c6cs00271d
13 Y. Zhu, H. Jia, G. Pan, N. W. Ulrich, Z. Chen and F. Wu, *J. Am. Chem. Soc.*, 2018, **140**, 4062–4070. https://doi.org/10.1021/jacs.7b13672
14 X. Yi, J. Dai, Y. Han, M. Xu, X. Zhang, S. Zhen, Z. Zhao, X. Lou and F. Xia, *Commun. Biol.*, 2018, **1**, 202. https://doi.org/10.1038/s42003-018-0204-6
15 A. P. Thomas, L. Palanikumar, M. T. Jeena, K. Kim and J.-H. Ryu, *Chem. Sci.*, 2017, **8**, 8351–8356. https://doi.org/10.1039/C7SC03169F
16 Z. Wang, F. Zhang, D. Shao, Z. Chang, L. Wang, H. Hu, X. Zheng, X. Li, F. Chen, Z. Tu, M. Li, W. Sun, L. Chen and W. Dong, *Adv. Sci.*, 2019, **6**, 1901690. https://doi.org/10.1002/advs.201901690
17 Y. Yuan, J. Liu and B. Liu, *Angew. Chem. Int. Ed.*, 2014, **53**, 7163–7168. https://doi.org/10.1002/anie.201402189
18 F. Zhang, Q. Ni, O. Jacobson, S. Cheng, A. Liao, Z. Wang, Z. He, G. Yu, J. Song, Y. Ma, G. Niu, L. Zhang, G. Zhu and X. Chen, *Angew. Chem. Int. Ed.*, 2018, **57**, 10564–10568. https://doi.org/10.1002/anie.201801984
19 D. Luo, K. A. Carter, A. Razi, J. Geng, S. Shao, D. Giraldo, U. Sunar, J. Ortega and J. F. Lovell, *Biomaterials*, 2016, **75**, 193–202. https://doi.org/10.1016/j.biomaterials.2015.10.027
20 B. Sun, C. Luo, W. Cui, J. Sun and Z. He, *J. Control. Release*, 2017, **258**, 281–294. https://doi.org/10.1016/j.jconrel.2017.08.034
21 J. Rautio, H. Kumpulainen, T. Heimbach, R. Oliyai, D. Oh, T. Järvinen and J. Savolainen, *Nat. Rev. Drug Discovery*, 2008, **7**, 255–270. https://doi.org/10.1038/nrd2468
22 Z. Fralish, A. Chen, S. Khan, P. Zhou and D. Reker, *Nat. Rev. Drug Discov.*, 2024, **23**, 365–380. https://doi.org/10.1038/s41573-024-00914-7
23 Z. Guo, J. Sui, M. Ma, J. Hu, Y. Sun, L. Yang, Y. Fan and X. Zhang, *J. Control. Release*, 2020, **326**, 350–364. https://doi.org/10.1016/j.jconrel.2020.07.030
24 D. Li, Y. Song, J. He, M. Zhang and P. Ni, *ACS Biomater. Sci. Eng.*, 2019, **5**, 2307–2315. https://doi.org/10.1021/acsbiomaterials.9b00301
25 J. Zhao, Y.-Y. Peng, D. Diaz-Dussan, J. White, W. Duan, L. Kong, R. Narain and X. Hao, *Mol. Pharmaceutics*, 2022, **19**, 1766–1777. https://doi.org/10.1021/acs.molpharmaceut.1c00518
26 W. Ke, N. Lu, A. A.-W. M. M. Japir, Q. Zhou, L. Xi, Y. Wang, D. Dutta, M. Zhou, Y. Pan and Z. Ge, *J. Control. Release*, 2020, **318**, 67–77. https://doi.org/10.1016/j.jconrel.2019.12.012
27 X. Xia, X. Yang, P. Huang and D. Yan, *ACS Appl. Mater. Interfaces*, 2020, **12**, 18301–18308. https://doi.org/10.1021/acsami.0c00650
28 J. Jiang, N. Shen, T. Ci, Z. Tang, Z. Gu, G. Li and X. Chen, *Adv. Mater.*, 2019, **31**, 1904278. https://doi.org/10.1002/adma.201904278
29 S. W. Chung, J. U. Choi, Y. S. Cho, H. R. Kim, T. H. Won, P. Dimitrion, O.-C. Jeon, S. W. Kim, I.-S. Kim, S. Y. Kim and Y. Byun, *Adv. Sci.*, 2018, **5**, 1800368. https://doi.org/10.1002/advs.201800368
30 X. Liu, Y. Li, K. Wang, Y. Chen, M. Shi, X. Zhang, W. Pan, N. Li and B. Tang, *Nano Lett.*, 2021, **21**, 7862–7869. https://doi.org/10.1021/acs.nanolett.1c03089
31 F. Sun, Q. Zhu, T. Li, M. Saeed, Z. Xu, F. Zhong, R. Song, M. Huai, M. Zheng, C. Xie, L. Xu and H. Yu, *Adv. Sci.*, 2021, **8**, 2002746. https://doi.org/10.1002/advs.202002746
32 P. Verwilst, J. Han, J. Lee, S. Mun, H.-G. Kang and J. S. Kim, *Biomaterials*, 2017, **115**, 104–114. https://doi.org/10.1016/j.biomaterials.2016.11.023
33 L. Ge, C. Qiao, Y. Tang, X. Zhang and X. Jiang, *Nano Lett.*, 2021, **21**, 3218–3224. https://doi.org/10.1021/acs.nanolett.1c00488
34 L. Liao, J. Liu, E. C. Dreaden, S. W. Morton, K. E. Shopsowitz, P. T. Hammond and J. A. Johnson, *J. Am. Chem. Soc.*, 2014, **136**, 5896–5899. https://doi.org/10.1021/ja502011g
35 L. Zhao, J. Peng, Q. Huang, C. Li, M. Chen, Y. Sun, Q. Lin, L. Zhu and F. Li, *Adv. Funct. Mater.*, 2014, **24**, 363–371. https://doi.org/10.1002/adfm.201302133
36 W. B. Direrssa, G. Getachew, C.-H. Hsiao, A. Wibrianto, A. S. Rasal, C.-C. Huang and J.-Y. Chang, *Mater. Today Chem.*, 2022, **26**, 101158. https://doi.org/10.1016/j.mtchem.2022.101158
37 G. Getachew, C.-H. Hsiao, A. Wibrianto, A. S. Rasal, W. B. Direrssa, C.-C. Huang, N. V. Rao, J.-H. Chen and J.-Y. Chang, *J.*

*Colloid Interface Sci.*, 2023, **633**, 396–410. https://doi.org/10.1016/j.jcis.2022.11.112
38 W. B. Direrса, G. Getachew, A. Wibrianto, A. S. Rasal, V. S. Gurav, M. Z. Fahmi and J.-Y. Chang, *J. Colloid Interface Sci.*, 2023, **647**, 528–545. https://doi.org/10.1016/j.jcis.2023.05.099
39 S. Huo, P. Zhao, Z. Shi, M. Zou, X. Yang, E. Warszawik, M. Loznik, R. Göstl and A. Herrmann, *Nat. Chem.*, 2021, **13**, 131–139. https://doi.org/10.1038/s41557-020-00624-8
40 B. A. Versaw, T. Zeng, X. Hu and M. J. Robb, *J. Am. Chem. Soc.*, 2021, **143**, 21461–21473. https://doi.org/10.1021/jacs.1c11868
41 C. Wang, Z. Zhang and Z. Liu, *ACS Cent. Sci.*, 2025, **11**, 1306–1320. https://doi.org/10.1021/acscentsci.5c00875
42 Y. Li, T. Gong, H. Gao, Y. Chen, H. Li, P. Zhao, Y. Jiang, K. Wang, Y. Wu, X. Zheng and W. Bu, *Angew. Chem. Int. Ed.*, 2021, **60**, 15472–15481. https://doi.org/10.1002/anie.202103015
43 J. Geng, Y. Zhang, Q. Gao, K. Neumann, H. Dong, H. Porter, M. Potter, H. Ren, D. Argyle and M. Bradley, *Nat. Chem.*, 2021, **13**, 805–810. https://doi.org/10.1038/s41557-021-00711-4
44 G. Liu, G. Zhang, J. Hu, X. Wang, M. Zhu and S. Liu, *J. Am. Chem. Soc.*, 2015, **137**, 11645–11655. https://doi.org/10.1021/jacs.5b05060
45 M. Y. Jiang and D. Dolphin, *J. Am. Chem. Soc.*, 2008, **130**, 4236–4237. https://doi.org/10.1021/ja800140g
46 R. R. Nani, A. P. Gorka, T. Nagaya, H. Kobayashi and M. J. Schnermann, *Angew. Chem. Int. Ed.*, 2015, **54**, 13635–13638. https://doi.org/10.1002/anie.201507391
47 P. Thapa, M. Li, M. Bio, P. Rajaputra, G. Nkepang, Y. Sun, S. Woo and Y. You, *J. Med. Chem.*, 2016, **59**, 3204–3214. https://doi.org/10.1021/acs.jmedchem.5b01971
48 G. Yang, X. Sun, J. Liu, L. Feng and Z. Liu, *Adv. Funct. Mater.*, 2016, **26**, 4722–4732. https://doi.org/10.1002/adfm.201600722
49 M. Bio, P. Rajaputra, G. Nkepang and Y. You, *J. Med. Chem.*, 2014, **57**, 3401–3409. https://doi.org/10.1021/jm5000722
50 C. G. Dariva, J. F. J. Coelho and A. C. Serra, *J. Control. Release*, 2019, **294**, 337–354. https://doi.org/10.1016/j.jconrel.2018.12.042
51 M. Jiang, J. Mu, O. Jacobson, Z. Wang, L. He, F. Zhang, W. Yang, Q. Lin, Z. Zhou, Y. Ma, J. Lin, J. Qu, P. Huang and X. Chen, *ACS Nano*, 2020, **14**, 847–857. https://doi.org/10.1021/acsnano.0c05722
52 V. Brega, F. Scaletti, X. Zhang, L.-S. Wang, P. Li, Q. Xu, V. M. Rotello and S. W. Thomas III, *ACS Appl. Mater. Interfaces*, 2018, **10**, 41274–41282. https://doi.org/10.1021/acsami.8b18099
53 X. Hu, Z. Qureishi and S. W. Thomas III, *Chem. Mater.*, 2017, **29**, 2979–2987. https://doi.org/10.1021/acs.chemmater.6b05294
54 L. Xu, Y. Yang, M. Zhao, W. Gao, H. Zhang, S. Li, B. He and Y. Pu, *J. Mater. Chem. B,* 2018, **6**, 1849–1857. https://doi.org/10.1039/C7TB02479G
55 B. Chu, Y. Qu, X. He, Y. Hao, C. Yang, Y. Yang, D. Hu, F. Wang and Z. Qian, *Adv. Funct. Mater.,* 2020, **30**, 2005918. https://doi.org/10.1002/adfm.202005918
56 X. Xu, P. E. Saw, W. Tao, Y. Li, X. Ji, S. Bhasin, Y. Liu, D. Ayyash, J. Rasmussen, M. Huo, J. Shi and O. C. Farokhzad, *Adv. Mater.*, 2017, **29**, 1700141. https://doi.org/10.1002/adma.201700141
57 W. Yin, W. Ke, W. Chen, L. Xi, Q. Zhou, J. F. Mukerabigwi and Z. Ge, *Biomaterials*, 2019, **195**, 63–74. https://doi.org/10.1016/j.biomaterials.2018.12.032
58 P. Pei, C. Sun, W. Tao, J. Li, X. Yang and J. Wang, *Biomaterials*, 2019, **188**, 74–82. https://doi.org/10.1016/j.biomaterials.2018.10.010
59 B. Liu and S. Thayumanavan, *Cell Rep. Phys. Sci.*, 2020, **1**, 100271. https://doi.org/10.1016/j.xcrp.2020.100271
60 W. Wang, C. Zhu, B. Zhang, Y. Feng, Y. Zhang and J. Li, *J. Am. Chem. Soc.*, 2023, **145**, 16644–16653. https://doi.org/10.1021/jacs.3c04109
61 S. Zhu, K. Li, S. Qin, J. Lin and L. Qiu, *J. Photochem. Photobiol. A: Chem.*, 2023, **439**, 114641. https://doi.org/10.1016/j.jphotochem.2023.114641
62 Q. Sun, Z. Zhou, N. Qiu and Y. Shen, *Adv. Mater.*, 2017, **29**, 1606628. https://doi.org/10.1002/adma.201606628
63 M. J. Mitchell, M. M. Billingsley, R. M. Haley, M. E. Wechsler, N. A. Peppas and R. Langer, *Nat. Rev. Drug Discov.*, 2021, **20**, 101–124. https://doi.org/10.1038/s41573-020-0090-8
64 P. Kumari, S. Jain, B. Ghosh, V. Zorin and S. Biswas, *Mol. Pharm.*, 2017, **14**, 3667–3677. https://doi.org/10.1021/acs.molpharmaceut.7b00468
65 L. Brannon-Peppas and J. O. Blanchette, *Adv. Drug Deliv. Rev.*, 2012, 64, 206–212. https://doi.org/10.1016/j.addr.2012.09.033
66 S. Li and L. Huang, *Mol. Pharm.*, 2008, **5**, 496–504. https://doi.org/10.1021/mp800049w
67 L. Yuan, Q. Chen, J. E. Riviere and Z. Lin, *J. Drug Deliv. Sci. Technol.*, 2023, **83**, 104404. https://doi.org/10.1016/j.jddst.2023.104404
68 T. Pham, V. Nguyen, Y. Choi, S. Lee and J. Yoon, *Chem. Rev.*, 2021, **121**, 13454–13619. https://doi.org/10.1021/acs.chemrev.1c00381
69 L. Liu, W. Qiu, B. Li, C. Zhang, L. Sun, S. Wan, L. Rong and X. Zhang, *Adv. Funct. Mater.*, 2016, **26**, 6257–6269. https://doi.org/10.1002/adfm.201602541
70 Y. Liu, T. Pauloehrl, S. I. Presolski, L. Albertazzi, A. R. A. Palmans and E. W. Meijer, *J. Am. Chem. Soc.*, 2015, **137**, 13096–13105. https://doi.org/10.1021/jacs.5b08299
71 S. Kim, M. Fujitsuka and T. Majima, *J. Phys. Chem. B*, 2013, **117**, 13985–13992. https://doi.org/10.1021/jp406638g
72 M. S. Cartiera, K. M. Johnson, V. Rajendran, M. J. Caplan and W. M. Saltzman, *Biomaterials*, 2009, **30**, 2790–2798. https://doi.org/10.1016/j.biomaterials.2009.01.057
73 J. J. Rennick, A. P. R. Johnston and R. G. Parton, *Nat. Nanotechnol.*, 2021, **16**, 266–276. https://doi.org/10.1038/s41565-021-00858-8
74 C. Flors, M. J. Fryer, J. Waring, B. Reeder, U. Bechtold, P. M. Mullineaux, S. Nonell, M. T. Wilson and N. R. Baker, *J. Exp. Bot.*, 2006, **57**, 1725–1734. https://doi.org/10.1093/jxb/erj181
75 A. Gomes, E. Fernandes and J. L. F. C. Lima, *J. Biochem. Biophys. Methods*, 2005, **65**, 45–80. https://doi.org/10.1016/j.jbbm.2005.10.003
76 T. Chou, *Pharmacol. Rev.*, 2006, **58**, 621–681. https://doi.org/10.1124/pr.58.3.10
77 L. Palanikumar, S. Al-Hosani, M. Kalmouni, V. P. Nguyen, L. Ali, R. Pasricha, F. N. Barrera and M. Magzoub, *Commun. Biol.*, 2020, **3**, 95. https://doi.org/10.1038/s42003-020-0817-4
78 J. Fujii, Y. Soma and Y. Matsuda, *Molecules*, 2023, **28**, 4085. https://doi.org/10.3390/molecules28104085
79 M. Przygoda, D. Bartusik-Aebisher, K. Dynarowicz, G. Cieślar, A. Kawczyk-Krupka and D. Aebisher, *Int. J. Mol. Sci.*, 2023, **24**, 16890. https://doi.org/10.3390/ijms242316890
80 Y. Pommier, *Nat. Rev. Cancer*, 2006, **6**, 789–802. https://doi.org/10.1038/nrc1977

View Article Online
DOI: 10.1039/D6MA00384B

The data supporting this article have been included as part of the Supplementary Information.

Supplementary information: experimental details, supporting figures, synthetic procedures, UV-vis, fluorescence, HPLC, and
NMR spectra.